

AD-A131 215

THE ANISOTROPY OF HIGH LATITUDE NIGHTTIME F-REGION
IRREGULARITIES(U) SRI INTERNATIONAL MENLO PARK CA
R C LIVINGSTON ET AL. 31 MAR 82 DNA-TR-81-87

1//

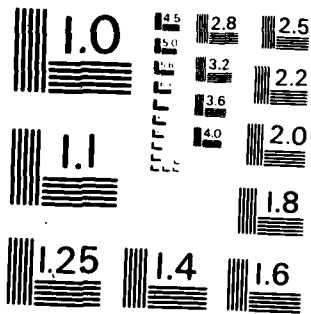
UNCLASSIFIED

DNA001-81-C-0076

F/G 4/1

NL

END
DATE
FILMED
DTIC



MICROCOPY RESOLUTION TEST CHART
NATIONAL BUREAU OF STANDARDS-1963-A

12

DNA TR-81-87

THE ANISOTROPY OF HIGH LATITUDE NIGHTTIME F-REGION IRREGULARITIES

ADA 131215

Robert C. Livingston
Roland T. Tsunoda
Charles L. Rino
Jacqueline Owen

SRI International
333 Ravenswood Avenue
Menlo Park, California 94025

31 March 1982

Technical Report

CONTRACT No. DNA 001-81-C-0076

APPROVED FOR PUBLIC RELEASE;
DISTRIBUTION UNLIMITED.

THIS WORK WAS SPONSORED BY THE DEFENSE NUCLEAR AGENCY
UNDER RDT&E RMSS CODE B322081466 S99QAXHC00022 H2590D.

DTIC FILE COPY

Prepared for
Director
DEFENSE NUCLEAR AGENCY
Washington, DC 20305

DTIC
ELECTE
AUG 10 1983
S B D

Destroy this report when it is no longer
needed. Do not return to sender.

PLEASE NOTIFY THE DEFENSE NUCLEAR AGENCY,
ATTN: STTI, WASHINGTON, D.C. 20305, IF
YOUR ADDRESS IS INCORRECT, IF YOU WISH TO
BE DELETED FROM THE DISTRIBUTION LIST, OR
IF THE ADDRESSEE IS NO LONGER EMPLOYED BY
YOUR ORGANIZATION.



UNCLASSIFIED

SECURITY CLASSIFICATION OF THIS PAGE (When Data Entered)

REPORT DOCUMENTATION PAGE		READ INSTRUCTIONS BEFORE COMPLETING FORM
1. REPORT NUMBER DNA-TR-81-87	2. GOVT ACCESSION NO.	3. RECIPIENT'S CATALOG NUMBER
4. TITLE (and Subtitle) THE ANISOTROPY OF HIGH LATITUDE NIGHTTIME F-REGION IRREGULARITIES		5. TYPE OF REPORT & PERIOD COVERED Technical Report
		6. PERFORMING ORG. REPORT NUMBER SRI Project 2623
7. AUTHOR(s) Robert C. Livingston Charles L. Rino Jacqueline Owen Roland T. Tsunoda		8. CONTRACT OR GRANT NUMBER(s) DNA 001-81-C-0076
9. PERFORMING ORGANIZATION NAME AND ADDRESS SRI International 333 Ravenswood Avenue Menlo Park, California 94025		10. PROGRAM ELEMENT, PROJECT, TASK AREA & WORK UNIT NUMBERS Task S99QAXHC-00022
11. CONTROLLING OFFICE NAME AND ADDRESS Director Defense Nuclear Agency Washington, D.C. 20305		12. REPORT DATE 31 March 1982
		13. NUMBER OF PAGES 34
14. MONITORING AGENCY NAME & ADDRESS (if different from Controlling Office)		15. SECURITY CLASS (of this report) UNCLASSIFIED
		15a. DECLASSIFICATION DOWNGRADING SCHEDULE N/A since UNCLASSIFIED
16. DISTRIBUTION STATEMENT (of this Report) Approved for public release; distribution unlimited.		
17. DISTRIBUTION STATEMENT (of the abstract entered in Block 20, if different from Report)		
18. SUPPLEMENTARY NOTES This work was sponsored by the Defense Nuclear Agency under RDT&E RMSS Code B322081466 S99QAXHC00022 H2590D.		
19. KEY WORDS (Continue on reverse side if necessary and identify by block number) Propagation Theory Scintillation Radio Waves Wideband Satellite		
20. ABSTRACT (Continue on reverse side if necessary and identify by block number) The anisotropy of intermediate-scale, F-region irregularities in the nighttime auroral zone is described. The study is based upon spaced- receiver phase-scintillation measurements made with the Wideband satellite at Poker Flat, Alaska. A systematic dependence of irregularity anisotropy with local time and magnetic latitude is observed, suggesting convective control. Sheet-like irregularities are confined to the zone of east-west		

DD FORM 1473
1 JAN 73

EDITION OF 1 NOV 65 IS OBSOLETE

UNCLASSIFIED

SECURITY CLASSIFICATION OF THIS PAGE (When Data Entered)

UNCLASSIFIED

SECURITY CLASSIFICATION OF THIS PAGE(When Data Entered)

20. ABSTRACT (continued)

drift near the equatorward boundary of the auroral zone. At the flow reversal, or Harang discontinuity, the cross-field extension of the sheets is reduced. The extension of rod-like irregularities, which are observed poleward of the zonal convection boundary, also shows apparent convection dominance. Mechanisms for convection control of the anisotropy are discussed.

UNCLASSIFIED

SECURITY CLASSIFICATION OF THIS PAGE(When Data Entered)

EXECUTIVE SUMMARY

High-latitude scintillation data from the DNA Wideband satellite show a conspicuous enhancement that arises from F-region irregularities with a high degree of spatial coherence in the plane of the local L shell. This phenomenon is of interest to the Defense Nuclear Agency for three reasons:

- (1) Convective instabilities, which are thought to generate these irregularities, are also believed to be operative in late-time nuclear environments.
- (2) Propagation disturbances are greatly enhanced along paths that coincide with axes or planes of enhanced spatial coherence.
- (3) Irregularities in the auroral zone, which can be transported over large distances, are strongly affected by the highly conducting auroral E layer.

In this report we present the first detailed analysis of the general anisotropy of nighttime auroral-zone irregularities obtained from spaced-receiver measurements. Spaced-receiver measurements are the only means of unambiguously resolving the irregularity anisotropy. Most of the previous work has relied on identifying systematic enhancement of the amplitude or phase scintillation or both.

The results of our analysis show systematic variations of irregularity anisotropy with invariant magnetic latitude and magnetic time. The sheet-like irregularities are confined to the zone of east-west auroral-zone convection. Moreover, at the transition or Harang discontinuity, the sheet-like anisotropy gives way to structures that have a much smaller cross-field anisotropy. Variations in the rod-like anisotropy outside the east-west convection zone also show systematic variations that point to convection, and associated velocity shears, as the cause of the anisotropy variations.

TABLE OF CONTENTS

<u>Section</u>	<u>Page</u>
EXECUTIVE SUMMARY	1
LIST OF ILLUSTRATIONS	3
I INTRODUCTION	5
II AURORAL ZONE ANISOTROPY	8
III ANISOTROPY MORPHOLOGY	17
IV DISCUSSION	21
REFERENCES	25

I INTRODUCTION

The anisotropy of small-scale, electron-density irregularities is an important factor both in systems design and instability theory. From basic principles, irregularities are expected to be elongated along magnetic field lines because of the high-parallel conductivity. On the other hand, the various instability mechanisms that cause those irregularities are quite complex. Experimentally, radio-wave diagnostics are the only practical means of quantitatively measuring irregularity anisotropy.

Radio-wave scintillation is enhanced whenever the propagation path lies within a plane or along a line of enhanced irregularity spatial coherence [Briggs and Parkin, 1963; Singleton, 1970; Rino and Fremouw, 1977]. This expected systematic enhancement for rod-like irregularities has been observed in midlatitude scintillation measurements [Bowhill, 1974]. At high latitudes, however, a systematic enhancement also appears whenever the propagation path lies within the local L shell. To explain this phenomenon, Martin and Aarons [1977] postulated a second axis of enhanced spatial-coherence transverse to the magnetic field along the local L shell. The individual irregularities can then be considered sheet-like, rather than rod-like structures.

Localized scintillation enhancements are prominent features in individual data records from the polar-orbiting Wideband satellite [Fremouw et al., 1977; Rino and Matthews, 1980; Fremouw and Lansinger, 1981a]. Moreover, through combined satellite and incoherent-scatter radar observations, the source region of the scintillation has been identified [Vickrey et al., 1980], and a comprehensive theory is emerging [Ossakow and Chaturvedi, 1979; Chaturvedi and Ossakow, 1979; Keskinen and Ossakow, 1982]. The experimental and theoretical developments along this line have been reviewed by Rino and Vickrey [1982].

In this report we describe the first comprehensive spatial coherence measurements of irregularity anisotropy in the nighttime auroral zone. The data were obtained from spaced-receiver measurements made at the Poker Flat, Alaska, Wideband receiving station. For a detailed description of the overall experiment see Fremouw et al. [1978]. The spaced-receiver measurements have been analyzed to extract quantitative measures of the anisotropy of the diffraction pattern. These are subsequently compared to propagation model predictions to estimate the in situ anisotropy.

The overall structure and anisotropy of the ionospheric irregularities can be characterized by a three-dimensional autocorrelation function. In the simplest model, a surface of constant spatial correlation is a prolate spheroid. In that case, the diffracted field of a radio wave passing through the irregularities can be characterized in any plane by a two-dimensional spatial autocorrelation function with elliptical contours of constant correlation. By measuring the correlation ellipse and observing its variation with changing propagation geometry, we can determine the anisotropy parameters that characterize the in situ irregularities.

The power of the method stems from the fact that, although they can change the shape of the spatial correlation functions that characterize the amplitude and phase of the diffracted wave field significantly, diffraction effects do not change the anisotropy. In particular, anisotropy, unlike geometrical scintillation enhancements, is invariant to changes in the perturbation strength.

To characterize the correlation ellipse of the measured diffraction pattern, we have implemented a method suggested by Armstrong and Coles [1972], which uses the intersections and peaks of all possible cross- and autocorrelation functions. An overdetermined set of linear equations results, which is then solved for the anisotropy coefficients by using standard least-squares methods. To determine the anisotropy coefficients of the irregularities, a search through various in situ anisotropies in a phase-screen model is made until a good match with the data is

obtained. The details of the method are described in a separate paper [Rino and Livingston, 1982].

In the analysis, we deal with three generic types of irregularities. If the structures are extended only in the direction of the magnetic field, they are referred to as rods. These rods can be characterized in terms of an axial ratio, a , which is the average along-field dimension, normalized to the corresponding cross-field dimension. A convenient designation for the rods is, therefore, $a:1:1$. If the irregularities have a second symmetrical preferred axis of elongation, perpendicular to the field and along the L shell, they will be referred to as sheets designated $a:a:1$. Similarly oriented, but nonsymmetrical irregularities ($a:b:1$ where $a > b$), will be referred to as wings. It will be shown that for certain propagation geometries an unambiguous distinction can be made among these three types of anisotropy.

The maximum cross-field dimension against which a and b are normalized is dictated by the measurement frequency and the rate at which the irregularities pass through the propagation path. In the Wideband data used here, the dimension is roughly 1 to 2 km. As an aside, we note that although individual irregularities in this spatial scale range are below the resolution limit of the Chatanika radar, they may be detectable with the EISCAT system.

The anisotropy analysis and modeling procedure is outlined in Section II. The results, presented in Section III, indicate convection dominance of auroral-zone anisotropy. Possible mechanisms for this anisotropy control are discussed in Section IV.

II AURORAL ZONE ANISOTROPY

As noted in Section I, there is considerable evidence that scintillation-producing irregularities in the auroral zone are not simple rod-like structures. Martin and Aarons [1977], using data from Goose Bay and orbiting beacons, deduced an overall 8:4:1 anisotropy within the auroral zone. Fremouw and Lansinger [1981b], using Wideband data, arrived at a similar 8:5:1 value based upon Wideband satellite data collected between 1976 and 1978. Both analyses base their conclusions on the assumption that the average irregularity strength through the region of geometrical enhancement is uniform, whereby the changes in average scintillation strength are strictly geometrically induced.

Moorecroft and Arima [1972] were the first to determine anisotropy from spaced-receiver measurements in the auroral zone. They deduced sheet-like structures, but with a meridional north-south alignment. Rino and Livingston [1982] first observed the expected diffraction pattern for L-shell-aligned, sheet-like irregularities in the 1976 Wideband data from Poker Flat. These data were recorded during a low solar-flux period of the sunspot cycle. For the current analysis, we have used a more extensive set of measurements that were made in 1978 during significantly higher solar-flux conditions. It is now well established that the scintillation-producing irregularities of interest here are predominantly in the F region. Chatanika radar incoherent-scatter data taken coincidentally with many of the satellite passes, show distinct F-layer ionization particularly during the high portion of the solar cycle.

To demonstrate the procedure we have used to interpret the measured axial ratio and orientation angle parameters and to illustrate possible ambiguities in the interpretation of the data, we describe the analysis of three representative data sets in detail. The data sets are from moderate elevation, overhead, and low-elevation Wideband passes as

observed at Poker Flat. For reference, the F-region penetration points are mapped in Figure 1 for all three cases.

Figure 2 shows the data for the moderate elevation case, which starts at 1118 UT. Superimposed on the data are the model calculations for four irregularity types: isotropic irregularities, rods, wings, and sheets.

It is instructive to compare the model predictions with one another. Both the axial ratio and orientation angle variations show very distinct changes with time. The Wideband satellite orbit is such that all the nighttime passes are aligned in geomagnetic north-south direction in the vicinity of Poker Flat (Figure 1). Field-aligned rods, illuminated by the satellite when it is low on the horizon, produce a ground shadow that is highly extended (axial ratio $\gg 1$) in a magnetic north-south direction. On the other hand, sheets similarly produce a shadow that is nearly uniform in space (axial ratio ~ 1). This difference is clearly evident in Figure 2(b), early and late in the satellite pass. Near the point of L-shell alignment, however, the situation is reversed. The rods are now illuminated more nearly along their primary axis, and produce a collapsed east-west shadow (axial ratio ~ 1), while the sheets produce an elongated east-west shadow with a pattern axial ratio only slightly smaller than in situ (axial ratio > 1). For the isotropic irregularity predictions, the diffraction pattern axial ratios exceed unity because the along-field and cross-field irregularity axes are scanned at different rates.

Our procedure for matching the model to the data is as follows: For the first third of the pass (up to about 1121 UT or 0100 corrected local magnetic time) from the orientation angle data alone, the in situ irregularity shapes cannot be distinguished; however, the axial ratio data in this segment are best matched by isotropic irregularities or sheets. To the far south, beyond 1127 UT, the situation is similar, although the results from the fitting procedure are compromised by sparse data.

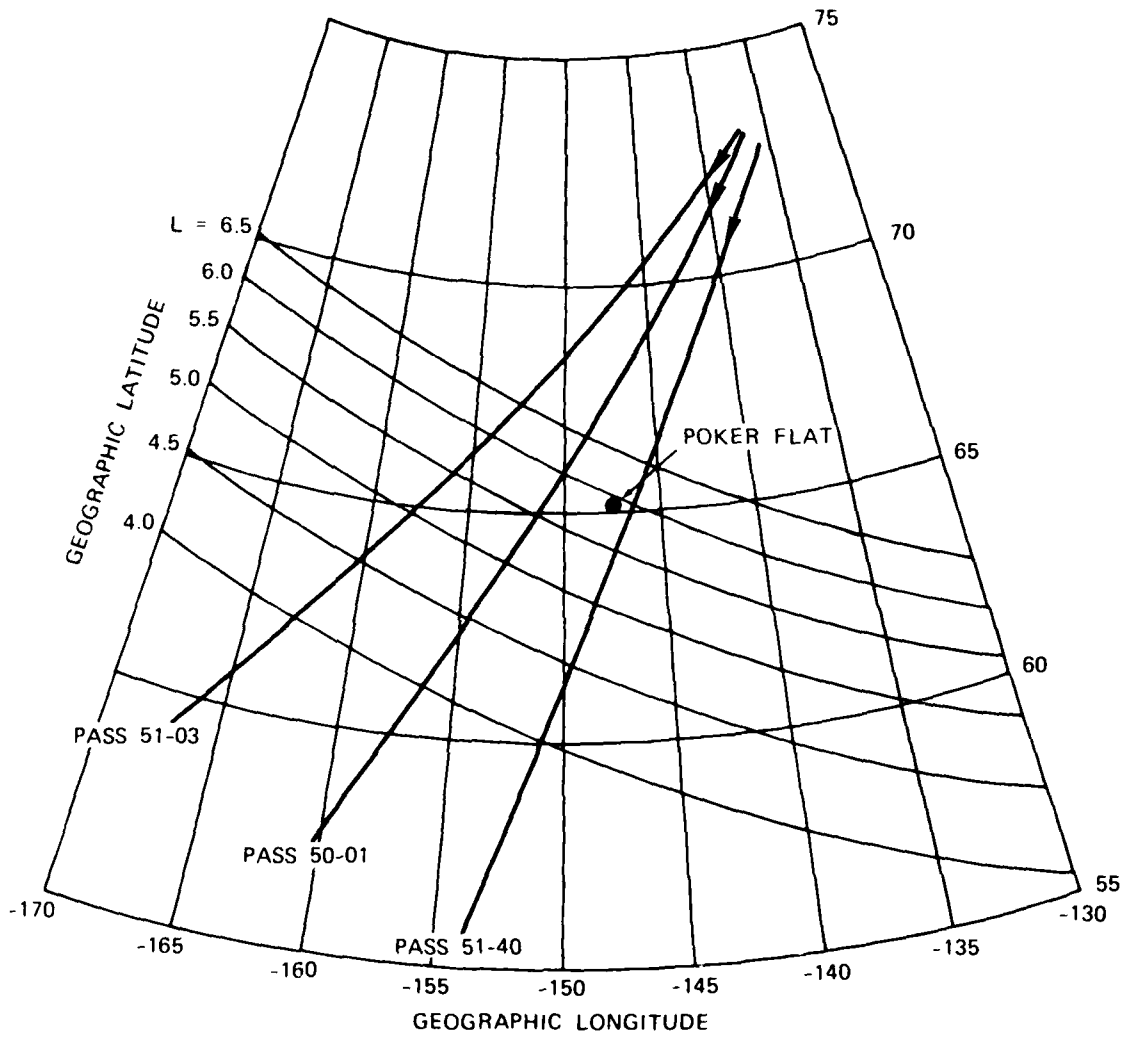


FIGURE 1 IONOSPHERIC PENETRATION POINT LOCATIONS (350 km) FOR THREE EXAMPLE PASSES

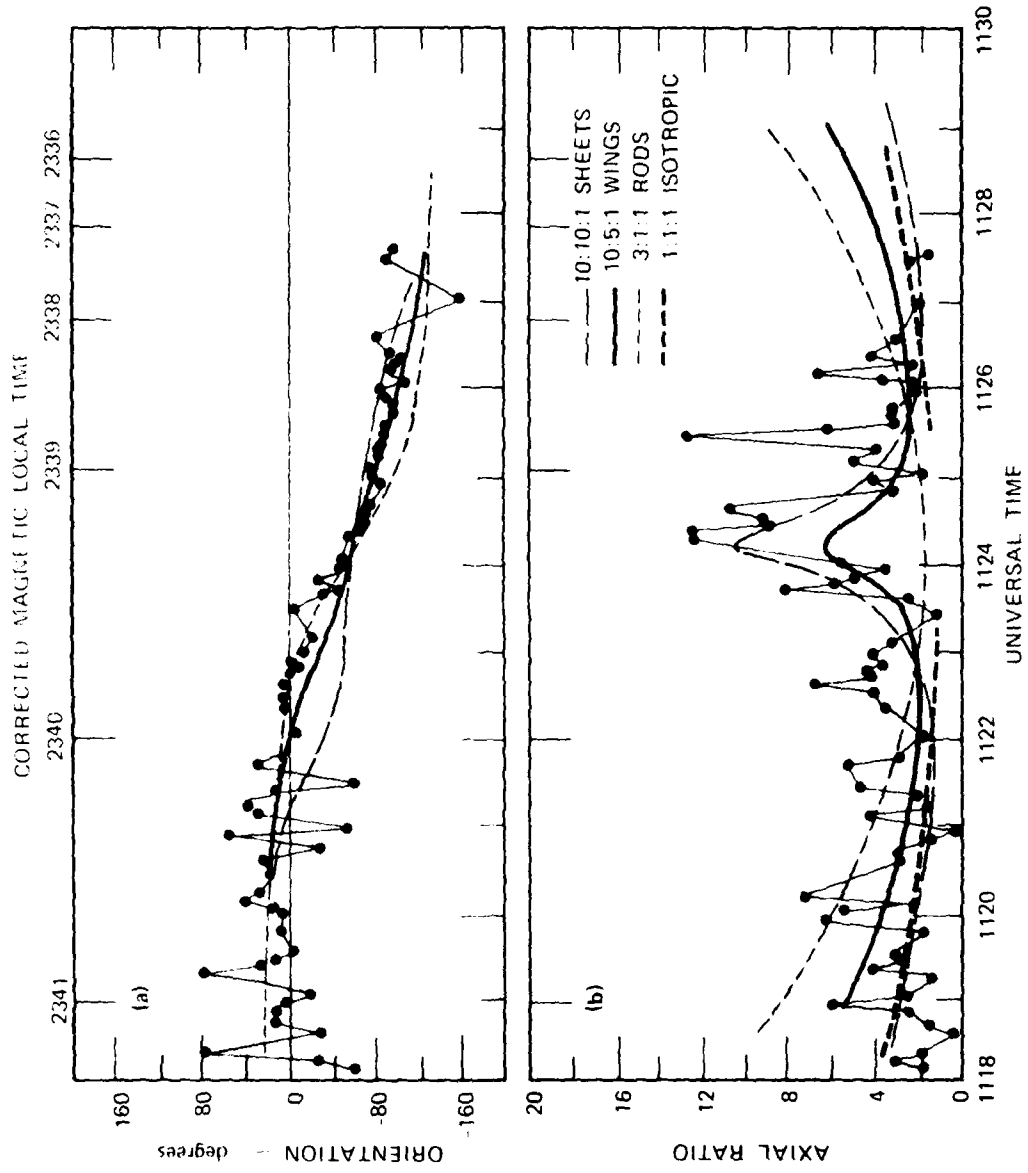


FIGURE 2 MEASURED AND MODEL ANISOTROPY VARIATION FOR MODERATE-ELEVATION POSTMIDNIGHT PASS (50-01)

In the center portion of the pass, there is a distinct enhancement in the measured axial ratio, near 1124 UT, which is matched well by a combination of the 10:5:1 wing and 10:10:1 sheet models. In this portion of the pass, the orientation angle data provide a more concise indicator of irregularity shape, and suggest that a progression of different anisotropies is being observed. Through 1123 UT, the irregularities are rod-like; near 1124 UT, the irregularity types cannot be clearly distinguished in orientation, although the axial ratio data suggest wings or sheets or both; beyond 1124:30 UT, the orientation data definitely indicate wings followed by sheets near 1126 UT.

Figure 3 shows the data from the nearly overhead pass. A high-elevation pass such as this provides maximum discrimination among the three types of in situ anisotropy types. As with the previous example, a mixture of rods, wings, and sheets seems to match the observed axial ratio data best, although, in this case, the anisotropy parameters that provide the best match are smaller than those deduced from the lower elevation passes. There is a point near 1033 UT at which the observed axial ratio becomes very large. All-sky photographs show that this enhancement corresponds to a bright, but stable arc. For our purposes of anisotropy morphology, it is only of passing interest.

Using both the axial ratio and orientation angle data, we can identify with some precision a sequence of irregularity types that are scanned as the satellite moves southward. Up through 1035 UT, the irregularities are evidently isotropic or low axial-ratio rods. The increase in observed axial ratio beyond 1035 UT indicates that the in situ irregularities are extended to about 5:1:1; the orientation angle clearly shows that they are rod-like in shape. Between 1036:40 and 1037:20, the axial ratio remains high, much as the sheet model would predict, but the orientation angle still indicates rods. Beyond this time, the orientation deviates from the rod signature to that for wings, and then to sheets. Thus, in this pass, as with Figure 2, we see an in situ irregularity anisotropy that is a function of latitude and shows a gradual transition from rods to sheets in a region to the south of Poker Flat.

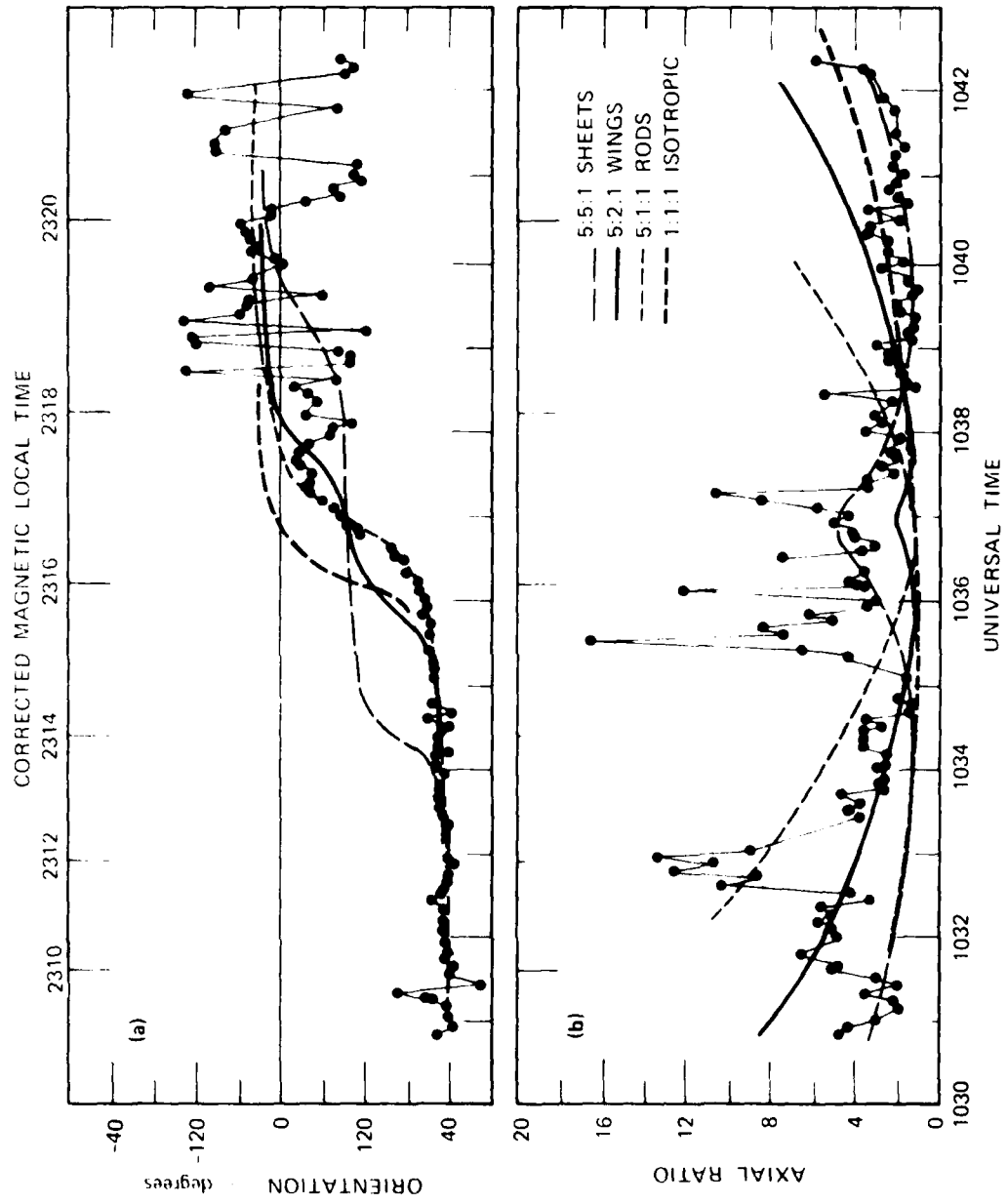


FIGURE 3 MEASURED AND MODEL ANISOTROPY VARIATION FOR HIGH-ELEVATION MIDNIGHT PASS (51-40)

As a third example, we have chosen a low-elevation pass, recorded ~ 90 min after local magnetic midnight. The F-region intercept is well to the west of Poker Flat. For such a geometry, the sheet and rod signatures remain distinctly different in axial ratio, but are too similar in orientation angle to allow the types of structures to be unambiguously differentiated.

Figure 4 shows the observed axial ratio and orientation angle for the low-elevation pass. Up through 1215 UT, 5:1:1 rods match the data well. Beyond 1215 UT, the large axial ratio enhancement is matched very well using 10:10:1 sheets in the model. The orientation angle variations provide very little discrimination, but are consistent with this combination. There is some suggestion in the orientation data beyond 1219 UT that sheets occur south of the region of axial ratio enhancement.

An alternative explanation to the axial ratio variation in Figure 4 could be a sudden change in the in situ structure from 5:1:1 rods to the north, to 15:1:1 (or larger) rods near overhead. We argue that this is less likely than the rods-to-sheets progression. First, the rods-to-sheets progression occurs for other propagation geometries. Second, a scintillation level enhancement accompanies the axial ratio enhancement near 1217 UT, which rods alone could not produce.

In sorting the large volume of data that is summarized in the next section, we have followed the process illustrated in the three examples. In summary then, for the moderate-to-high elevation passes, for which the correlation surface orientation is very sensitive to changes in the model parameters, those data are used to identify the generic irregularity type: isotropic, rods, wings, or sheets. A fortunate and useful result is that for sheet extensions beyond about 3:3:1 and wings beyond about 4:2:1, the pattern of orientation-angle variations saturates and remains unchanged for further increases in a or b or both. For these same geometries, the axial ratio data are used to establish the actual degree of anisotropy for the various irregularity types. For the low-elevation passes, we depend almost entirely on the axial-ratio data, as our last example illustrated.

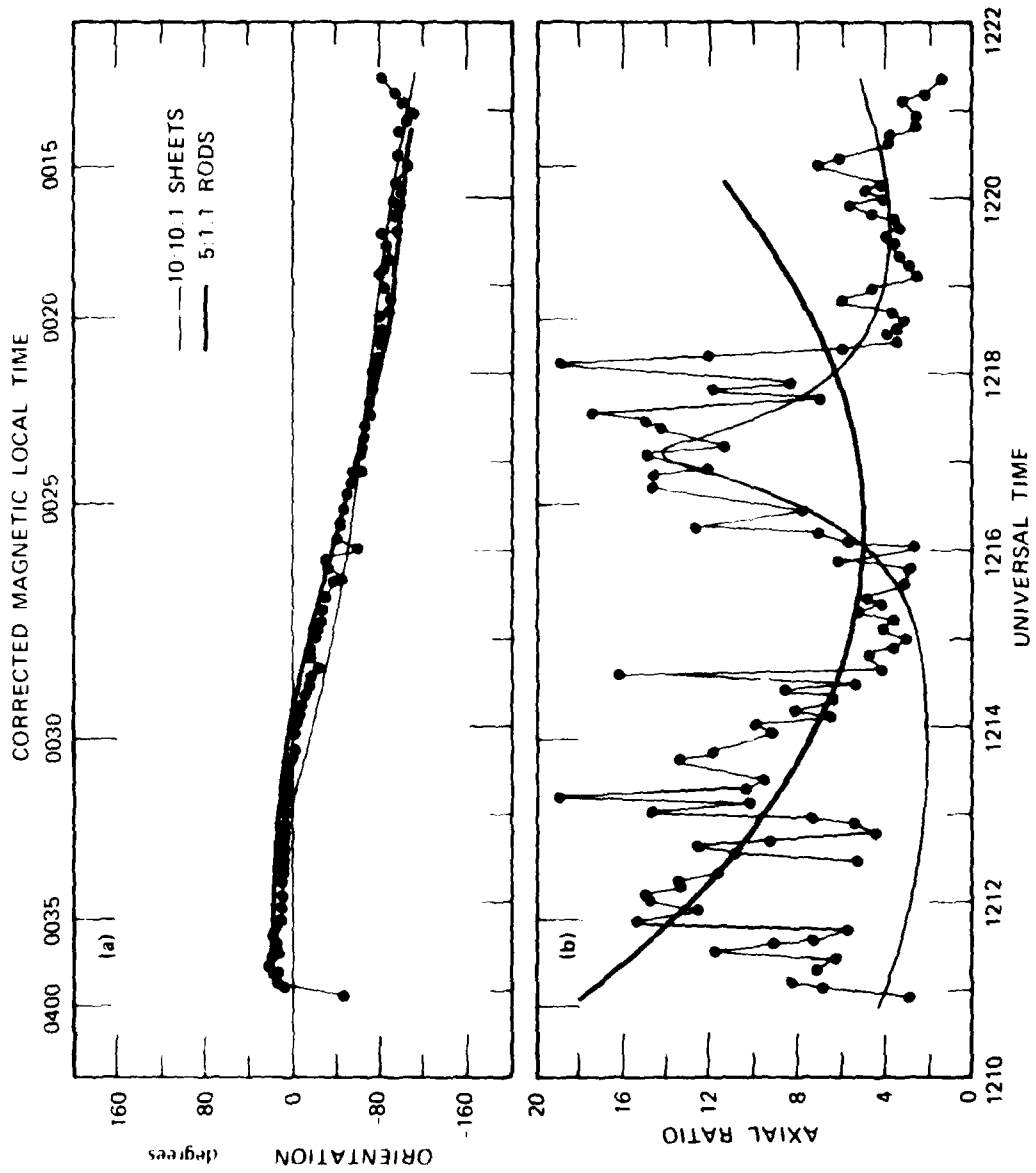


FIGURE 4 MEASURED AND MODEL ANISOTROPY VARIATION FOR LOW-ELEVATION POSTMIDNIGHT PASS (51-03)

A formal error analysis of the method used to extract axial ratio and orientation from the measurements has yet to be performed. It is a complicated task in its own right because of the number of functional manipulations involved. We guess that the error estimates for orientation would be small, based upon the consistency of that parameter over large portions of each pass. The point we wish to reinforce is that the method is sensitive enough that even without error bars, we can be confident in our identification of the generic irregularity: rods, wings, or sheets. Furthermore, even if the dimensions of each irregularity type cannot be precisely defined, the relative patterns of extension are unambiguous.

III ANISOTROPY MORPHOLOGY

Our anisotropy analysis was performed on data from a large number of nighttime passes collected during several weeks of observation made during February and March 1978. The anisotropy behavior for nights of weak magnetic disturbance ($K_p = 1$ to 2) have been consolidated in Figure 5. The data are plotted on a grid of invariant magnetic latitude and corrected magnetic local time for the 350-km altitude of propagation penetration. This format is convenient, since the anisotropy patterns may be related to auroral-zone dynamics. The locations of the start and end points of each pass are indicated by arrows.

The contoured portions of the map in Figure 5 indicate regions in which rod-like irregularities give the best overall fit to the data. The axial ratio parameter, a , is indicated. The contours include only the regions within which rods can be clearly identified, either from the orientation angle variation (for high-elevation look angles), or from measured axial ratios that are too high to be produced by sheets (at low-elevation look angles). North of the contoured area, the observed axial ratios are low enough to be produced by either isotropic irregularities or sheets, and the orientation angle data is ambiguous. Other evidence, however, suggests that the irregularities are nearly isotropic in this region. Measurements at Thule, Greenland, in the polar cap, collected for nearly the same season as the Poker Flat data, but at somewhat shorter cross-field spatial scale sizes, show low-anisotropic rods or isotropic irregularities.

The cross-hatched portions of Figure 5 indicate the regions for which sheets or wings give the best fit to the data. For all but the lowest-elevation angles, at early and late times, this identification is made using the measured orientation angle progression. The value of the in situ axial ratio, a , is estimated from the magnitude of the observed axial ratio. In some cases, e.g., when sheets and wings are

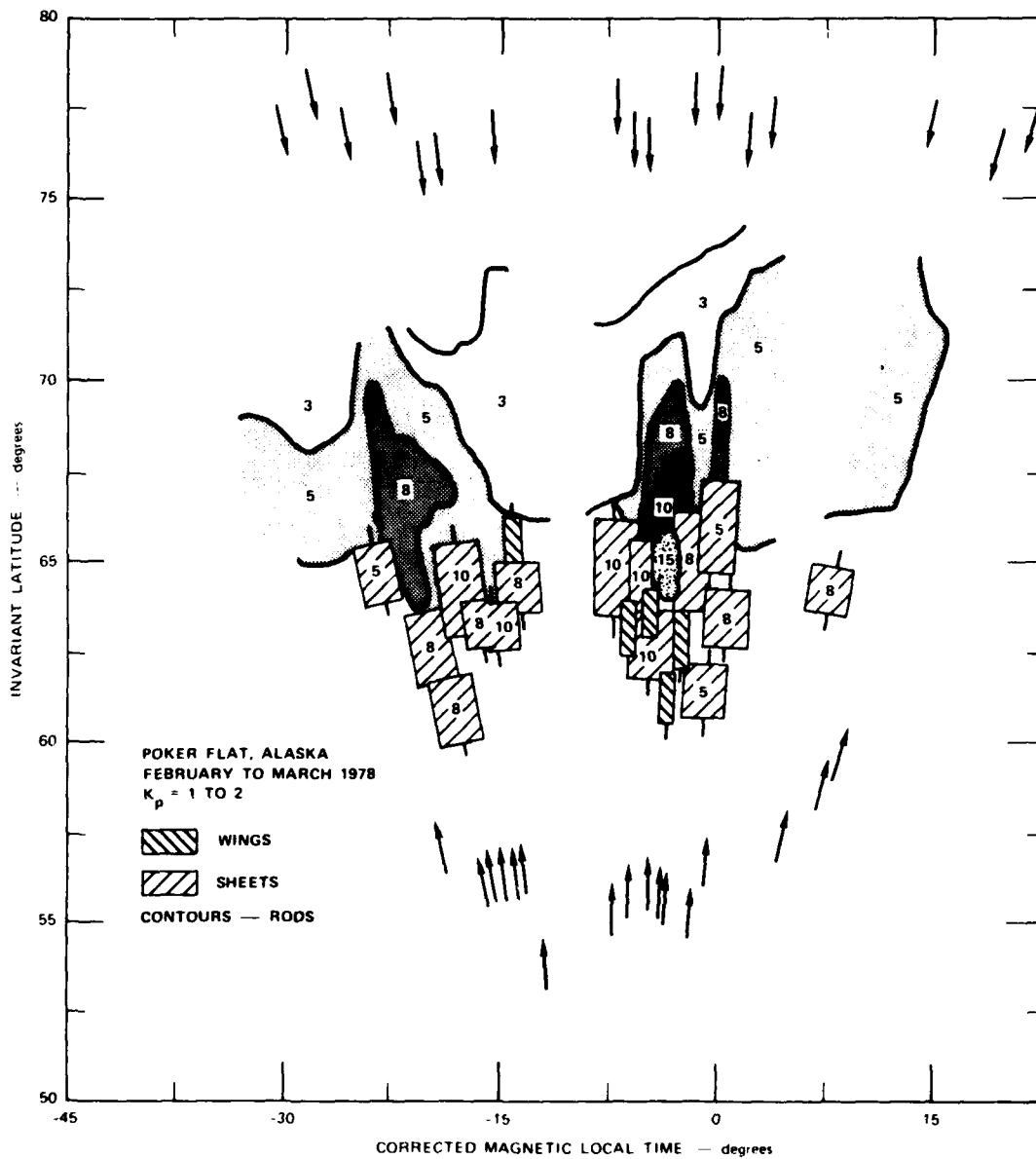


FIGURE 5 OVERALL ANISOTROPY PATTERN FOR QUIET MAGNETIC CONDITIONS

mixed and the sheets fall on the edge of the region of the predicted axial-ratio enhancement, the sheet dimension cannot be accurately defined. The sheet dimension is, then, assumed the same as that of the best-fit wing or wing/sheet combination. For simplicity in fitting the data, the wings are always assumed to have a cross-field dimension half that along the field.

At low-elevation look angles to the south of the wing/sheet region in Figure 5 is another region in which it is difficult to identify the irregularity type precisely. As was the case with the northernmost region, the low observed axial ratios and the lack of discrimination in orientation angle makes definite identification difficult. In the majority of cases, however, the orientation-angle progression leading into this region suggests that sheets are present. This region corresponds to the low-electron-density trough south of the auroral precipitation zone.

Figure 6 shows the overall anisotropy distribution in latitude-local time for moderate levels of magnetic-disturbance ($K_p = 3$ to 4). It provides a somewhat more uniform sampling of the anisotropy in local time, but is otherwise very similar in gross features to Figure 5.

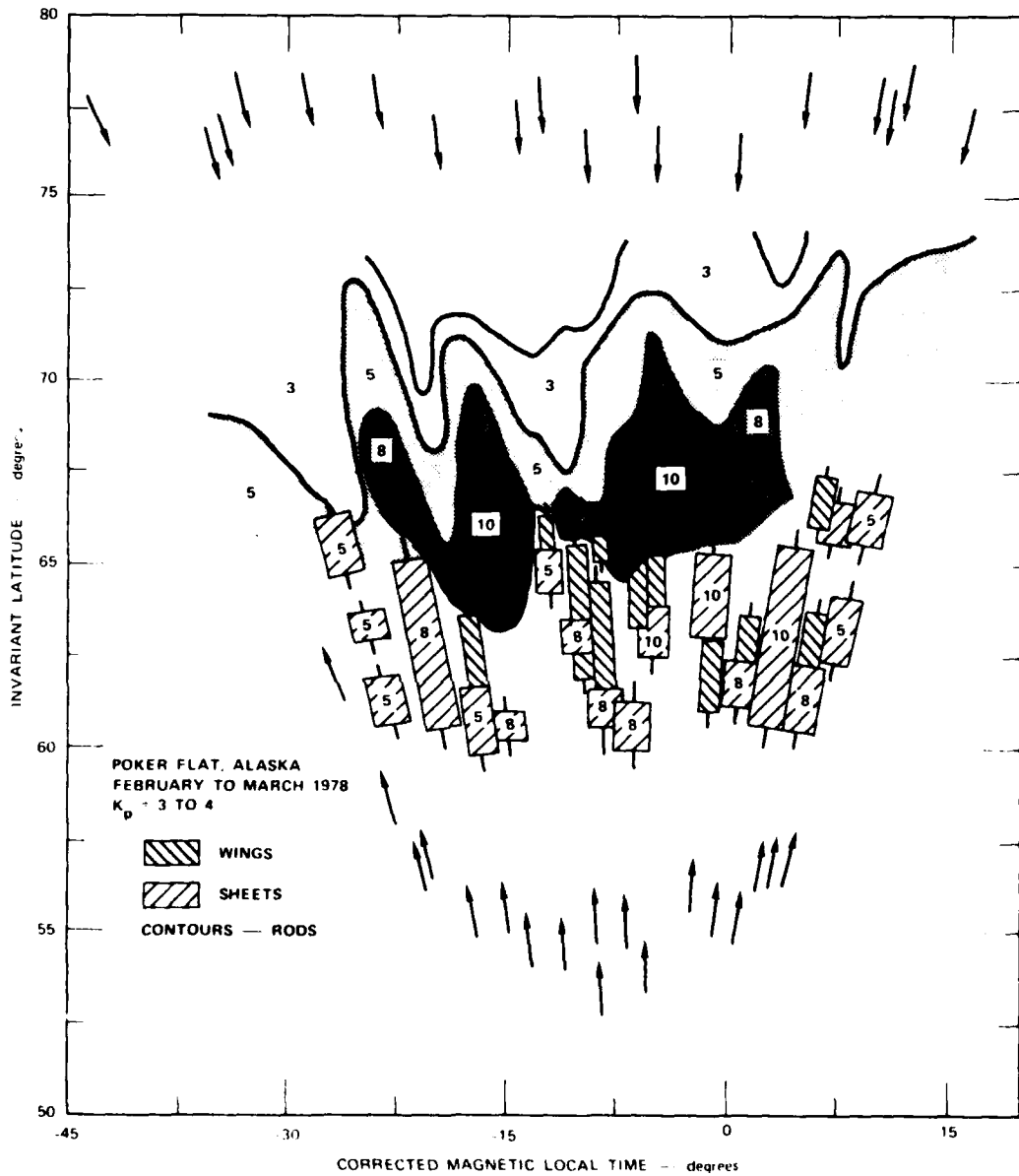


FIGURE 6 OVERALL ANISOTROPY PATTERN FOR MODERATE MAGNETIC CONDITIONS

IV DISCUSSION

In the data summarized in Figures 5 and 6, there are distinct systematic variations in in situ irregularity anisotropy. In the pre-midnight and postmidnight data, the north-to-south latitudinal progression is from nearly isotropic irregularities to rods with increasing elongation giving way to sheets that abruptly disappear at the scintillation boundary. Through the midnight sector the anisotropy is generally reduced. At latitudes at which rods are found, the axial ratio is reduced, and at latitudes at which sheets are found, the sheets give way to wings. This structuring suggests the well-known pattern of nighttime auroral-zone plasma convection, which Figure 7 shows schematically.

In Figure 7, the Harang discontinuity is the region in which the antisunward flow separates into westward and eastward drifts. We have shown the discontinuity as it is usually pictured, tilted in the latitude/local time frame [Heppner, 1972]. The time of occurrence of the discontinuity is a function of global magnetic-field conditions, as is, to some degree, its tilt and shape. The placement of the flow pattern in Figure 7 in both local time and latitude was chosen using the observations of Maynard [1972]. Using in situ drift data, he identified the Harang discontinuity under very quiet and disturbed conditions. Our moderate Kp conditions lie somewhere between these extremes. Perhaps as important, the boundary near 62-to-63° invariant latitude is also the expected equatorward edge of the auroral precipitation zone [Sheehan and Caravillano, 1978]. The distinct and stable F-region ionization buildup at this latitude is a conspicuous feature in the Chatanika radar data taken during the recent solar maximum [Vickrey et al., 1980]. Presumably, the ionization arises from long-term low-energy particle precipitation [Winningham et al., 1975]. Recent measurements have shown, moreover, that the ionization enhancements are structured east-west, at tens of kilometers and larger scales [Tsunoda and Vickrey, 1982].

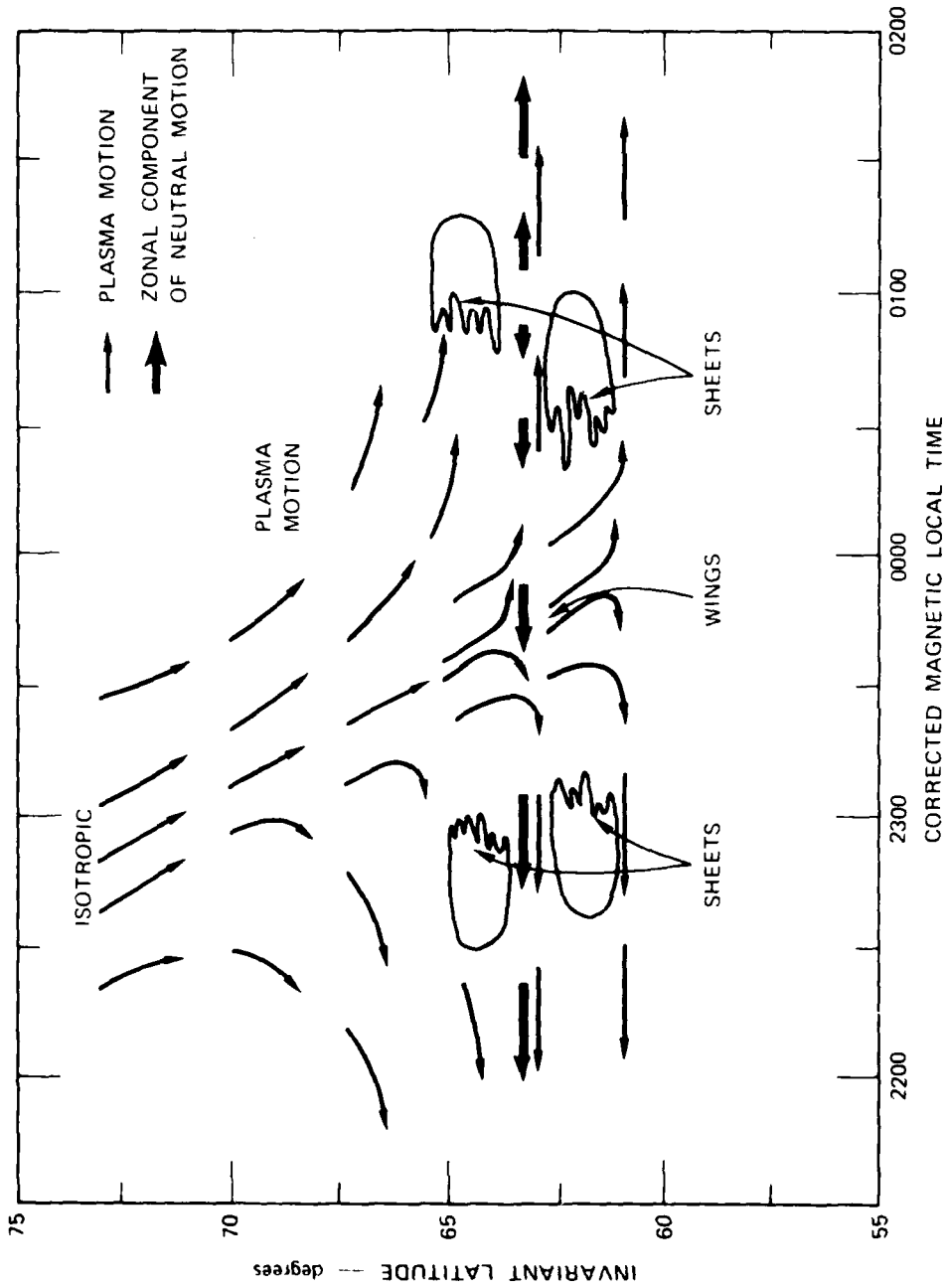


FIGURE 7 EXPECTED CONVECTIVE FLOW PATTERN FOR LOW-TO-MODERATE MAGNETIC CONDITIONS ILLUSTRATING POSSIBLE PLASMA STRUCTURING

The flow pattern in Figure 7, which is based on independent observations [Maynard, 1972], matches the anisotropy patterns in Figures 5 and 6. Proceeding from that model, we can use the first principles of convective instability theory to explain the detailed anisotropy behavior.

First, let us consider the rod-like irregularity regions in Figures 5 and 6. The contours are not symmetrical in local time, and the overall pattern is shifted roughly perpendicular to the tilt of the Harang discontinuity. In the poleward extension of the Harang discontinuity, the rods are extended the least, which suggests that the irregularities are being transported from the polar cap. The anisotropy maximizes immediately on either side of the Harang discontinuity, at which place the plasma velocity shear is maximum in both the zonal and meridional directions. These are also the regions in which the rods, which have been in the discontinuity flow for the longest time, are deposited. If during their transport, they are able to extract energy using a convective instability process, the dimensions of the rods are likely affected.

Within the auroral boundary region, the large-scale density enhancements observed by radar are prone to secondary instability structuring. In particular, the large northward and southward electric fields that occur pre- and postmidnight will cause any westward or eastward density gradient to be gradient-drift unstable. Such structuring could produce the sheet-like kilometer-scale irregularities that we observe, as schematically illustrated in Figure 7. The confinement of the sheets to the boundary region and the reduction of sheet-like anisotropy in the Harang discontinuity, as seen in Figures 5 and 6, fit this pattern well. The neutral wind also undoubtedly plays a role in the structuring process. Premidnight, the zonal component of neutral wind is a stabilizing force against the gradient drift instability, as shown in Figure 7. However, momentum delays the shift in neutral wind direction until well past midnight. This additional destabilization should make the postmidnight sheets more prominent than those observed premidnight, which also agrees with our data.

In summary, then, our observations strongly point towards convection dominance of kilometer-scale, F-region irregularity anisotropy. The specific structuring processes that we suggest need to be theoretically verified. Keskinen and Ossakow [1982] have recently demonstrated that large-scale east-west structuring of the auroral boundary can result from a process similar to the vertical Rayleigh Taylor structuring of the equatorial ionosphere. At much shorter scales, Chaturvedi and Ossakow [1979] have studied the current convective instability in the auroral zone. From numerical simulations such as these, at intermediate scales and from recent radar-scintillation measurement campaigns, details of the anisotropy process should soon emerge.

REFERENCES

- Armstrong, J. W. and W. A. Coles, "Analysis of Three Station Interplanetary Scintillation," J. Geophys. Res., 77(25), 4602-4610, (1972).
- Bowhill, S. A., "Satellite Transmission Studies of Spread-F Produced by Artificial Heating of the Ionosphere," Radio Sci., 9(11), 975-986, (1974).
- Briggs, B. H. and I. A. Parkin, "On the Variation of Radio Star and Satellite Scintillations with Zenith Angle," J. Atmos. Terr. Phys., 25(6), 339, (1963).
- Chaturvedi, P. K. and S. L. Ossakow, "Nonlinear Stabilization of the Current Convective Instability in the Diffuse Aurora," Geophys. Res. Lett., 6(12), 957-959, (1979).
- Fremouw, E. J. and J. M. Lansinger, "Dominant Configurations of Scintillation-Producing Irregularities in the Auroral Zone," J. Geophys. Res., 86(A12), 10087-10092, (1981a).
- Fremouw, E. J., and J. M. Lansinger, "A Computer Model for High-Latitude Phase Scintillation Based on Wideband Satellite Data from Poker Flat," DNA Report 5686F, Contract No. DNA001-79-C-0372, Physical Dynamics, Inc., Bellevue, WA (1981b).
- Fremouw, E. J., R. L. Leadabrand, R. C. Livingston, M. D. Cousins, C. L. Rino, B. C. Fair and R. A. Long, "Early Results from the DNA Wideband Satellite Experiment--Complex Signal Scintillation," Radio Sci., 13(1), 167-187, (1978).
- Heppner, J. P., "The Harang Discontinuity in Auroral-Belt Ionospheric Currents," Geophys. Publ., 29, 105-120, (1972).
- Keskinen, M. J. and S. L. Ossakow, "Nonlinear Evolution of Plasma Enhancements in the Auroral Ionosphere: 1. Long Wavelength Irregularities," J. Geophys. Res., 87(A1), 144-150, (1982).
- Martin, E. and J. Aarons, "F-Layer Scintillations and the Aurora," J. Geophys. Res., 82(19), 2717-2722, (1977).
- Maynard, N. C., "Electric-Field Measurements Across the Harang Discontinuity," J. Geophys. Res., 79(31), 4620-4631, (1974).

- Moorecroft, D. R. and K. S. Arima, "The Shape of the F-Region Irregularities, Which Produce Satellite Scintillations--Evidence for Axial Symmetry," J. Atmos. Terr. Phys., 34(3), 437-450, (1972).
- Ossakow, S. L. and P. K. Chaturvedi, "Current Convective Instability in the Diffuse Aurora," Geophys. Res. Lett., 6(4), 322-334, (1979).
- Rino, C. L. and E. J. Fremouw, "The Angle Dependence of Singly Scattered Wavefields," J. Atmos. Terr. Phys., 39(8), 859-868, (1977).
- Rino, C. L. and R. C. Livingston, "On the Analysis and Interpretation of Spaced-Receiver Measurements of Transionospheric Radio Waves," Radio Sci., accepted for publication, 1982.
- Rino, C. L. and S. J. Matthews, "On the Morphology of Auroral Zone Radio-Wave Scintillation," J. Geophys. Res., 85(A8), 4139-4151, (1980).
- Rino, C. L. and J. F. Vickrey, "Recent Results in Auroral-Zone Scintillation Studies," submitted for publication, 1982.
- Sheehan, R. E. and A. L. Caravillano, "Characteristics of the Equatorward Auroral Boundary Near Midnight Determined from DMSP Images," J. Geophys. Res., 83(A10), 4799-4754, (1978).
- Singleton, D. G., "The Effect of Irregularity Shape on Radio Star and Satellite Scintillations," J. Atmos. Terr. Phys., 32(2), 315-343, (1970).
- Tsunoda, R. T. and J. F. Vickrey, "Evidence of East-West Structure in Large-Scale F-Region Plasma Enhancements," submitted for publication, 1982.
- Vickrey, J. F., C. L. Rino, and T. A. Potemra, "Chatanika/Triad Observations of Unstable Ionization Enhancements in the Auroral F-Region," Geophys. Res. Lett., 7(10), 789-792, (1980).
- Winningham, J. D., F. Yasuhara, S. I. Akasofu, and W. J. Heikkila, "The Latitudinal Morphology of 10-eV to 10-keV Electron Fluxes During Magnetically Quiet and Disturbed times in the 2100-0300 MLT Sector," J. Geophys. Res., 80(22), 3148-3171, (1975).

DISTRIBUTION LIST

DEPARTMENT OF DEFENSE

Command & Control Technical Center
 ATTN: C-312, R. Mason
 ATTN: C-650, G. Jones
 3 cy ATTN: C-650, W. Heidig

Defense Communications Agency
 ATTN: Code 230
 ATTN: Code 205
 ATTN: J300 for Yen-Sun Fu

Defense Communications Engineer Center
 ATTN: Code R123
 ATTN: Code R410, N. Jones

Defense Intelligence Agency
 ATTN: DB-4C, E. O'Farrell
 ATTN: DC-7B
 ATTN: DB, A. Wise
 ATTN: DT-1B
 ATTN: DIR

Defense Nuclear Agency
 ATTN: STNA
 ATTN: NAFD
 ATTN: RAEI
 ATTN: NATD
 ATTN: RAAI, P. Lunn
 3 cy ATTN: RAAI
 4 cy ATTN: TITL

Defense Technical Information Center
 10 cy ATTN: DD

Dep. Under Secretary of Defense
 Com. Cnd. Cont & Intell
 ATTN: Dir of Intelligence Sys

Field Command
 Defense Nuclear Agency, Det 1
 Lawrence Livermore Lab
 ATTN: FC-1

Field Command
 Defense Nuclear Agency
 ATTN: FCTT, W. Summa
 ATTN: FCPR
 ATTN: FCTXE
 ATTN: FCTT, G. Ganong

Interservice Nuclear Weapons School
 ATTN: TTY

Joint Chiefs of Staff
 ATTN: C3S
 ATTN: C3S, Evaluation Office (H000)

Joint Strat Tgt Planning Staff
 ATTN: JLTW-2
 ATTN: JLA, Threat Applications Div

National Security Agency
 ATTN: B-3, F. Leonard
 ATTN: R-52, J. Skillman
 ATTN: W-32, O. Bartlett

DEPARTMENT OF DEFENSE (Continued)

Under Secy of Def for Resch & Engrg
 ATTN: Strat & Theater Nuc Forces, B. Stephan
 ATTN: Strategic & Space Sys (OS)

WMCCS System Engineering Org
 ATTN: J. Hoff

DEPARTMENT OF THE ARMY

Assistant Chief of Staff for Automation & Comm
 ATTN: DAMO-C4, P. Kenny

Atmospheric Sciences Laboratory
 ATTN: DELLAS-EO, F. Niles

BMD Advanced Technology Center
 ATTN: ATC-R, D. Russ
 ATTN: ATC-R, W. Dickinson

BMD Systems Command
 ATTN: BMDSC-HLI, R. Webb
 2 cy ATTN: BMDSC-HW

Dep. Chief of Staff for Ops & Plans
 ATTN: DAMO-RQC, C2 Div

Harry Diamond Laboratories
 ATTN: DELHD-NW-P
 ATTN: DELHD-NW-R, R. Williams

US Army Chemical School
 ATTN: ATZN-CM-CS

US Army Comm-Elec Engrg Instal Agency
 ATTN: CCC-CEI-CCO, W. Neuendorf
 ATTN: CCC-EMEC-PED, G. Lane

US Army Communications Command
 ATTN: CC-OPS-WR, H. Wilson
 ATTN: CC-OPS-W

US Army Communications R&D Command
 ATTN: DRDCO-COM-RY, W. Kesselman

US Army Foreign Science & Tech Ctr
 ATTN: DRXST-SD

US Army Materiel Dev & Readiness Cnd
 ATTN: DRCLDC, J. Bender

US Army Nuclear & Chemical Agency
 ATTN: Library

US Army Satellite Comm Agency
 ATTN: Document Control

US Army TRADOC Sys Analysis Actvy
 ATTN: ATAA-PL
 ATTN: ATAA-TCC, F. Payan, Jr
 ATTN: ATAA-TDC

DEPARTMENT OF THE NAVY

Joint Cruise Missiles Project Ofc
ATTN: JCMG-707

Naval Air Systems Command
ATTN: PMA 271

Naval Electronic Systems Command
ATTN: PME 117-2013, G. Burnhart
ATTN: PME 117-20
ATTN: PME 106-13, T. Griffin
ATTN: PME 117-211, B. Kruger
ATTN: PME 106-4, S. Kearney
ATTN: Code 3101, T. Hughes
ATTN: Code 931A

Naval Intelligence Support Ctr
ATTN: NISC-90

Naval Research Laboratory
ATTN: Code 4733
ATTN: Code 4700
ATTN: Code 4700, J. Davis
ATTN: Code 7900, B. Wald
ATTN: Code 4187
ATTN: Code 6700
ATTN: Code 7950, J. Goodman

Naval Space Surveillance System
ATTN: J. Burton

Naval Surface Weapons Center
ATTN: Code F31

Naval Telecommunications Command
ATTN: Code 341

Ofc of the Deputy Chief of Naval Ops
ATTN: OP 931N
ATTN: OP 941D
ATTN: N0F 654, Strat Eval & Anal Br

Office of Naval Research
ATTN: Code 412, W. Condell
ATTN: Code 414, G. Joiner

Strategic Systems Project Office
ATTN: NSP-2722, F. Wimberly
ATTN: NSP-141
ATTN: NSP-43

Theater Nuclear Warfare Proj Office
ATTN: PM-23, D. Smith

DEPARTMENT OF THE AIR FORCE

Aerospace Defense Command
ATTN: DC, T. Long

Air Force Geophysics Laboratory
ATTN: PHY, J. Buchau
ATTN: DPR-1
ATTN: LRB, K. Champion
ATTN: CA, A. Stair
ATTN: R. Babcock
ATTN: R. O'Neil

Rome Air Development Center
ATTN: ELP, J. Rasmussen

DEPARTMENT OF THE AIR FORCE (Continued)

Air Force Weapons Laboratory
ATTN: D01
ATTN: NTYC
ATTN: NTN

Air Force Wright Aeronautical Lab
ATTN: W. Hunt
ATTN: R. Johnson

Air Logistics Command
ATTN: DO-ALCMM

Air University Library
ATTN: ALL-LEI

Assistant Chief of Staff
Studies & Analysis
ATTN: AF SASC, C. Rieghtover
ATTN: AF SASC, W. Kraus

Ballistic Missile Office
ATTN: SAC, Col Swan
ATTN: TNSA, W. Wilson

Deputy Chief of Staff
Research, Development, & Acq
ATTN: AFROD, Colonel W. C. Orr
ATTN: AFROD
ATTN: AFROD

Deputy Chief of Staff
Operational and Plans
ATTN: AFOP
ATTN: AFOP
ATTN: AFOP

Electronic Warfare Div
ATTN: C-1, Col Clark

Electronic Warfare Division
ATTN: EWT-4, Col Jones

Electronic Systems Division
ATTN: NSD-2, Lt Col Arnold
ATTN: LCS-1E

Foreign Technology Division
ATTN: NTS Library
ATTN: TQTD, B. Ballard

Rome Air Development Center
ATTN: QCS, V. Payne
ATTN: TNSD

Space Division
ATTN: YGCB, W. Mercer
ATTN: YKM, Maj Alexander
ATTN: YKM, Cpt Norton

Strategic Air Command
ATTN: DCNA, T. Jensen
ATTN: NRC
ATTN: APFS
ATTN: DCY

OTHER GOVERNMENT AGENCIES

Central Intelligence Agency
ATTN: OSWR SSD for K. Feuerpfell

Department of Commerce
National Bureau of Standards
ATTN: Sec Ofc for R. Moore

Department of Commerce
National Oceanic & Atmospheric Admin
ATTN: R. Grubb

Institute for Telecommunications Sciences
ATTN: W. Utlaut
ATTN: L. Berry
ATTN: A. Jean

DEPARTMENT OF ENERGY CONTRACTORS

EG&G, Inc
Los Alamos Division
ATTN: J. Colvin
ATTN: D. Wright

University of California
Lawrence Livermore National Lab
ATTN: Technical Info Dept Library

Los Alamos National Laboratory
ATTN: C. Westervelt
ATTN: P. Keaton

Sandia National Lab
ATTN: Org 1250, W. Brown
ATTN: D. Thornbrough
ATTN: Space Project Div
ATTN: Teen Lib 3141
ATTN: D. Dahlgren

Sandia National Labs, Livermore
ATTN: T. Cook
ATTN: B. Murphy

DEPARTMENT OF DEFENSE CONTRACTORS

Aerospace Corp
ATTN: D. Olsen
ATTN: V. Josephson
ATTN: T. Saffi
ATTN: I. Garfunkel
ATTN: R. Slaughter
ATTN: J. Straus

Analytical Systems Engineering Corp
ATTN: Radio Sciences

Analytical Systems Engineering Corp
ATTN: Security

BOM Corp
ATTN: T. Neighbors
ATTN: L. Jacobs

Berkeley Research Associates, Inc
ATTN: S. Brecht
ATTN: J. Workman

DEPARTMENT OF DEFENSE CONTRACTORS (Continued)

Boeing Co
ATTN: S. Tashird
ATTN: G. Hall

Booz-Allen & Hamilton, Inc
ATTN: B. Wilkinson

BR Communications
ATTN: J. McLaughlin

University of California at San Diego
ATTN: H. Booker

Charles Stark Draper Lab, Inc
ATTN: D. Cox
ATTN: A. Tetewski
ATTN: J. Gilmore

Computer Sciences Corp
ATTN: F. Eisenbarth

Comsat Labs
ATTN: D. Fang
ATTN: G. Hyde

Cornell University
ATTN: M. Kelly
ATTN: D. Farley, Jr

E-Systems, Inc
ATTN: R. Berezdin

Electrospace Systems, Inc
ATTN: H. Logston

EOS Technologies, Inc
ATTN: B. Gabbard

ESL, Inc
ATTN: J. Marshall

General Electric Co
ATTN: A. Steinmayer
ATTN: C. Zierdt

General Electric Co
ATTN: G. Millman

General Research Corp
ATTN: B. Bennett

Honeywell, Inc
ATTN: G. Terry, Avionics Dept
ATTN: G. Collyer, Avionics Dept

Horizons Technology, Inc
ATTN: R. Kruger

HSS, Inc
ATTN: D. Hansen

IBM Corp
ATTN: H. Ulander

DEPARTMENT OF DEFENSE CONTRACTORS (Continued)

Institute for Defense Analyses
ATTN: J. Aein
ATTN: H. Wolfhard
ATTN: E. Bauer

International Tel & Telegraph Corp
ATTN: Technical Library

International Tel & Telegraph Corp
ATTN: G. Wetmore

JAYCOR
ATTN: J. Sperling

JAYCOR
ATTN: J. DonCarlos

Johns Hopkins University
ATTN: J. Phillips
ATTN: T. Evans
ATTN: J. Newland
ATTN: P. Komiske

Kaman Sciences Corp
ATTN: T. Stephens

Kaman Tempo
ATTN: B. Gambill
ATTN: J. Devore
ATTN: DASIAC
ATTN: K. Schwartz
ATTN: W. Knapp

Litton Systems, Inc
ATTN: B. Zimmer

Lockheed Missiles & Space Co, Inc
ATTN: J. Kumer
ATTN: R. Sears

Lockheed Missiles & Space Co, Inc
ATTN: D. Churchill, Dept 81-11
ATTN: Dept 60-12
ATTN: C. Old, Dept 66-21

M.I.T. Lincoln Lab
ATTN: D. Towle

MA'COM Linkabit Inc
ATTN: A. Viterbi
ATTN: I. Jacobs
ATTN: H. Van Trees

Magnavox Govt & Indus Electronics Co
ATTN: G. White

McDonnell Douglas Corp
ATTN: H. Spitzer
ATTN: W. Olson

Meteor Communications Corp
ATTN: R. Leader

Mitre Corp
ATTN: A. Kymnel
ATTN: G. Harding
ATTN: C. Callahan
ATTN: B. Adams

DEPARTMENT OF DEFENSE CONTRACTORS (Continued)

Mission Research Corp
ATTN: R. Bigoni
ATTN: S. Gutsche
ATTN: F. Fajen
ATTN: F. Guigliano
ATTN: Tech Library
ATTN: R. Hendrick
ATTN: R. Bogusch
ATTN: C. Lauer
ATTN: G. McCartor

Mitre Corp
ATTN: M. Horrocks
ATTN: W. Foster
ATTN: W. Hall

Pacific-Sierra Research Corp
ATTN: E. Field, Jr
ATTN: F. Thomas
ATTN: H. Brode, Chairman SAGE

Pennsylvania State University
ATTN: Ionospheric Research Lab

Photometrics, Inc
ATTN: I. Kofsky

Physical Dynamics, Inc
ATTN: E. Fremouw

Physical Research, Inc
ATTN: R. Deliberis

R&D Associates
ATTN: R. Lelevier
ATTN: F. Gilmore
ATTN: M. Gantsweg
ATTN: C. Greifinger
ATTN: R. Turco
ATTN: H. Ory
ATTN: W. Karzas
ATTN: W. Wright

R&D Associates
ATTN: B. Yoon

Rand Corp
ATTN: E. Bedrozian
ATTN: C. Crain

Riverside Research Institute
ATTN: V. Trapani

Rockwell International Corp
ATTN: R. Buckner

Rockwell International Corp
ATTN: S. Quilici

Santa Fe Corp
ATTN: D. Paolucci

Science Applications, Inc
ATTN: L. Linson
ATTN: E. Straker
ATTN: D. Hamlin
ATTN: C. Smith

DEPARTMENT OF DEFENSE CONTRACTORS (Continued)

SRI International
ATTN: G. Smith
ATTN: M. Baron
ATTN: D. Neilson
ATTN: R. Leadabrand
ATTN: W. Jaye
ATTN: W. Chesnut
ATTN: G. Price
ATTN: A. Burns
ATTN: J. Petrickes
4 cy ATTN: R. Tsunoda
4 cy ATTN: R. Livingston
4 cy ATTN: C. Rino
4 cy ATTN: J. Owen

Stewart Radiance Laboratory
ATTN: J. Ulwich

Sylvania Systems Group
ATTN: R. Steinhoff

Sylvania Systems Group
ATTN: I. Kohlberg

DEPARTMENT OF DEFENSE CONTRACTORS (Continued)

Tri-Com, Inc
ATTN: D. Murray

TRw Electronics & Defense Sector
ATTN: G. Kirchner
ATTN: D. Dee
ATTN: R. Plebuch

Utah State University
Attention: Sec Control Ofc for
ATTN: L. Jensen, Elec Eng Dept
ATTN: A. Steed
ATTN: K. Baker, Dir Atmos & Space Sci
ATTN: D. Furt

Visidyne, Inc
ATTN: J. Carpenter
ATTN: O. Shepard
ATTN: W. Reidy

LME
— 8